Pergamon

Int. J. Solids Structures Vol. 33, No. 25, pp. 3755–3777, 1996

0020-7683/96 $15.00 + .00

0020-7683(95)00205-7

EDGE DEBONDING IN PATCHED CYLINDRICAL PANELS

W. J. BOTTEGA and M. A. LOIA
Department of Mechanical and Aerospace Engineering, Rutgers University, Piscataway, NJ 08855-0909 U.S.A.

(*Received* 12 *January* 1995; *in revised form* 23 *August* 1995)

Abstract—Circumferential edge debonding is considered for structural configurations corresponding to patched cylindrical panels, under a variety of loading conditions. These include applied circumferential tension, radial three-point loading, and applied pressure. The effect of support conditions on the evolution of the composite structure is also examined as are the effects of relative stiffness and arc length of the patch with respect to those of the base panel. The problems are approached from a unified point of view, as a moving interior boundaries problem in the calculus of variations, resulting in a selfconsistent model of the intact and debonded segments of the composite structure, the individual primitive structures, and the corresponding conditions which define the intermediate boundaries of the bonded region and a region of sliding contact. Numerical simulations based on analytical solutions reveal characteristic behavior of the evolving structure under load. Copyright © 1996 Elsevier Science Ltd

1. INTRODUCTION

A method of repair for damaged (cracked) structures which is receiving increased attention of late, particularly with regard to aircraft structures, is the adherence of a "patch" over the damaged surface in an attempt to transfer the load to the patch and thus alleviate the stress intensity in the vicinity of the damage. (See for example, Park *et al.*, 1992, or Baker, 1993.) Similar "piggy-back" configurations may occur, for example, in structures where a sensor/controller material layer has been bonded to the base structure or for adhesively bonded lap-joints. (See for example, Oplinger, 1994, and Tsai and Morton, 1994.) The question of debonding of the patch from the base structure is an issue, as the effectiveness of the overall structure may be compromised once debonding ensues.

Typically, the patch is designed and its effectiveness evaluated with regard to alleviating the in-plane stress intensity and load transfer by considering a plane stress type analysis for a flat structure (Baker, 1993, Chiu *et al.*, 1994, Chue *et al.*, 1994, Paul and Jones, 1992, Park *et al.*, 1992, Roderick, 1980, Sih and Hong, 1989, Tarn and Shek, 1991). In their papers, Sih and Hong (1989) considered the planar interaction of edge debonds and a thickness crack, as well, for the case of circular patches adhered to a flat panel, while Roderick (1980) and Baker (1993) also considered interior debonding in the vicinity of the crack in a patched flat panel. In addition, we note that the related problem of edge delamination in composites has also been studied to some extent (see, for example, Schellenkens and Borst, 1993). In a recent paper by Bottega (1995), the issue of edge debonding was considered for flat structures configured in the aforementioned manner. Specifically, the problems of edge debonding in patched plates and lap-joints were considered, where it was seen that out of plane bending together with in-plane stretching strongly influenced the debonding behavior of the evolving structure. Many characteristics of the debonding structure were demonstrated including the existence of a contact zone under certain conditions, the influence of support conditions on the debonding behavior, and the influence of the relative patch stiffness and length, among others.

As many actual structures possess nonvanishing curvature it would appear necessary to consider parallel studies for similarly configured curved structures. This is the subject of the present work. In particular we consider the problem of edge debonding in patched cylindrical panels for three types of loading conditions and a variety of support conditions

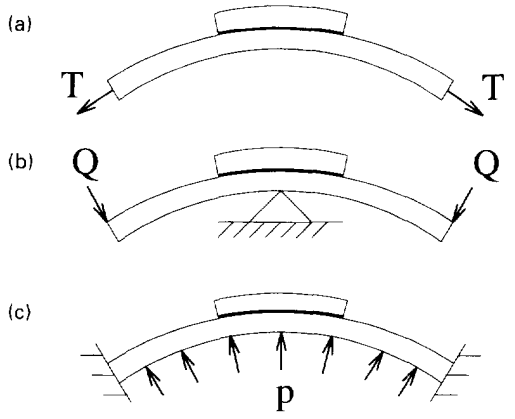

Fig. 1. Patched cylindrical panel under various loading conditions: (a) applied circumferential tension, (b) three-point radial loading, (c) applied pressure (shown with clamped-fixed supports).

which are the analogs of those considered by Bottega (1995) for patched plates. The loading types include (i) applied circumferential tension, (ii) radial three-point loading, and (iii) applied internal pressure loading (Fig. 1). It will be seen that while these structures exhibit many of the characteristics demonstrated by their flat counterparts, the curved structures do, however, behave differently. As in related studies (for example, Bottega, 1983, 1988, 1994, 1995, and Loia and Bottega, 1994) the problem is formulated from a unified point of view, as a moving intermediate boundaries problem in the calculus of variations—with a shallow shell theory used to model the base structure and the patch individually and a Griffith type energy criterion incorporated to govern debonding—yielding a self-consistent formulation for the evolving composite structure.

2. FORMULATION

Consider the thin cylindrical structure comprised of a base panel/shell of (angular) half-span Φ to which a cylindrical patch of half-span $\Phi_p \leqslant \Phi$ is adhered over the region S_1: $\theta \in [0, \alpha]$ as shown in Fig. 2, where θ is the angular coordinate measured from centerspan of the structure. Further, let us consider the debonded portion of the patch to maintain sliding contact over the region S_2: $\theta \in [\alpha, \beta]$ immediately ahead of the bonded region, while the portion of the patch defined on S_3: $\theta \in [\beta, \Phi]$ is lifted/separated from the base structure. These three regions will be referred to as the "bond zone", "contact zone" and "lift zone", respectively. The domain of definition of the portion of the patch in the lift zone is S_{3p}: $\theta \in [\beta, \Phi_p]$ such that $S_{3p} \subset S_3$. When referring to the portion of the patch in region S_3, it

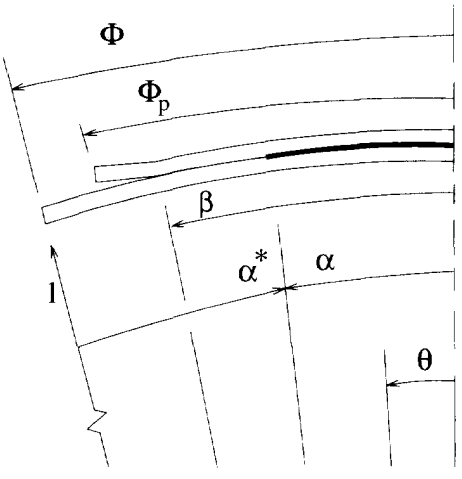

Fig. 2. Half span of panel showing characteristic lengths/angles and coordinates.

will be understood that the corresponding subregion is indicated. At this point, let us also define the "conjugate bond zone size" $\alpha^* \equiv \Phi - \alpha$ as indicated in the figure. We shall be interested in examining the evolution and response of the "composite structure" when it is subjected to (i) applied circumferential tension, (ii) three-point radial loading, and (iii) applied (internal) pressure. In what follows all length scales are normalized with respect to the dimensional radius R of the undeformed structure, and the common surface or interface between the patch and base panel, and its extension, will be used as the reference surface.

Both the base structure and the patch will be modeled using the shallow shell model employed in Bottega (1988a–d and 1994) and Loia and Bottega (1994). The corresponding relations for the normalized (centerline) membrane strains $e_i(\theta)$ and $e_{pi}(\theta)$ and the normalized curvature changes $\kappa_i(\theta)$ and $\kappa_{pi}(\theta)$ for the base structure and patch in each region are thus respectively given by

$$e_i = u_i' - w_i + \tfrac{1}{2}w_i'^2, \quad \kappa_i = w_i'' + w_i, \quad \theta \in S_i \tag{1a,b}$$

$$(i = 1, 2, 3)$$

$$e_{pi} = u_{pi}' - w_{pi} + \tfrac{1}{2}w_{pi}'^2, \quad \kappa_{pi} = w_{pi}'' + w_{pi}, \quad \theta \in S_{ip} \tag{1c,d}$$

In eqns (1a)–(1d), $u_i = u_i(\theta)$ (positive in direction of increasing θ) and $w_i = w_i(\theta)$ (positive inward) respectively correspond to the circumferential and radial displacements of the centerline of the base panel in region S_i, and $u_{pi} = u_{pi}(\theta)$ and $w_{pi} = w_{pi}(\theta)$ correspond to the analogous displacements of the centerline of the patch. In addition, superposed primes indicated total differentiation with respect to θ.

The displacements $u_i(\theta)$ and $u_{pi}(\theta)$ and the membrane strains $e_i(\theta)$ and $e_{pi}(\theta)$ of the substructure centerlines are related to their counterparts at the reference surface, $u_i^*(\theta)$ and $u_{pi}^*(\theta)$, and $e_i^*(\theta)$ and $e_{pi}^*(\theta)$, by the relations

$$u_i^* = u_i + \frac{h}{2}w_i', \quad u_{pi}^* = u_{pi} - \frac{h_p}{2}w_{pi}', \quad (i = 1, 2, 3) \tag{2a,b}$$

$$e_i^* = e_i + \frac{h}{2}\kappa_i, \quad e_{pi}^* = e_{pi} - \frac{h_p}{2}\kappa_{pi}, \quad (i = 1, 2, 3) \tag{3a,b}$$

where $h \ll 1$ and $h_p \ll 1$ correspond to the normalized thickness of the base panel and patch, respectively. At this point let us also introduce the normalized membrane stiffness C and bending stiffness D of the base panel, and the corresponding normalized membrane and bending stiffness, C_p and D_p, of the patch. The normalization of the stiffness of the primitive structures is based on the bending stiffness of the base panel and the radius R of the system in the undeformed configuration. Hence,

$$C = 12/h^2, \quad D = 1, \quad C_p = CE_0h_0, \quad D_p = E_0h_0^3, \tag{4a–d}$$

where:

$$h_0 = h_p/h, \quad E_0 = E_p/E \quad \text{or} \quad E_0 = \frac{E_p/(1-\nu_p^2)}{E/(1-\nu^2)}, \tag{4e,f}$$

E and E_p correspond to the (dimensional) elastic moduli of the base panel and patch, respectively, and ν and ν_p correspond to the associated Poisson's ratios.

Paralleling the developments in Bottega (1994 and 1995) we next formulate an energy functional in terms of (i) the strain energies of each of the individual segments of both the base panel and patch independently and expressed in terms of the reference surface variables, (ii) the work done by the applied loading for each case of interest, (iii) constant functionals which match the radial displacements in the contact zone, and both the radial and circumferential displacements in the bond zone (the Lagrange multipliers in this case correspond to the interfacial radial stress and interfacial radial and circumferential shear

stresses respectively), and (iv) a delamination energy functional corresponding to the energy required to create an arc length of new debond. We thus formulate an energy functional Π, as follows:

$$\Pi = \sum_{i=1}^{3} \{U_B^{(i)} + U_{Bp}^{(i)} + U_M^{(i)} + U_{Mp}^{(i)}\} - \Lambda - \mathscr{W} + \Gamma \tag{5}$$

where:

$$U_B^{(i)} = \int_{S_i} \tfrac{1}{2} D\kappa_i^2 \, d\theta, \quad U_{Bp}^{(i)} = \int_{S_i} \tfrac{1}{2} D_p \kappa_{pi}^2 \, d\theta, \quad (i = 1-3) \tag{6a,b}$$

respectively correspond to the bending energies of the base panel, and of the patch, in region i,

$$U_M^{(i)} = \int_{S_i} \tfrac{1}{2} C e_i^2 \, d\theta, \quad U_{Mp}^{(i)} = \int_{S_i} \tfrac{1}{2} C_p e_{pi}^2 \, d\theta, \quad (i = 1-3) \tag{7a,b}$$

are the corresponding membrane energies of the base panel and patch, respectively, Λ is a constraint functional, given by

$$\Lambda = \sum_{i=1}^{2} \left\{ \int_{S_i} \sigma_i (w_{pi} - w_i) \, d\theta \right\} + \int_{S_1} \tau (u_{p1}^* - u_1^*) \, d\theta, \tag{8a,b}$$

where $\sigma_i (i = 1, 2)$ and τ are Lagrange multipliers ($\sigma_2 < 0$), $\mathscr{W}$ corresponds to the work done by the applied loading and is given by

$$\mathscr{W} = T_0 u_3(1), \quad \text{or} \quad \mathscr{W} = Q_0 w_3(1), \quad \text{or} \quad \mathscr{W} = -\sum_{i=1}^{3} \left\{ \int_{S_i} p w_i \, d\theta \right\}, \tag{9a,b,c}$$

depending upon the specific problem of interest, where T_0 represents the normalized applied circumferential tension, Q_0 is the normalized intensity of the applied radial line/point loads for the 3-point case, and p corresponds to the normalized applied (internal) pressure. Further,

$$\Gamma = 2\gamma(\alpha^* - \alpha_0^*) \tag{10}$$

is the delamination energy,† where

$$\alpha^* = 1 - \alpha \tag{11}$$

is the "conjugate" bond zone (half) length as defined earlier, α_0^* corresponds to some initial value of α^*, and γ is the normalized bond energy (bond strength). The normalized loads T_0, Q_0, and p are related to their dimensional counterparts $\bar{T}$, $\bar{Q}$, and $\bar{p}$, by

$$T_0 = \bar{T} R^2 / \bar{D}, \quad Q_0 = \bar{Q} R^2 / \bar{D}, \quad p = \bar{p} R^3 / \bar{D},$$

where $\bar{D}$ is the dimensional bending stiffness of the base panel. In a similar manner, the normalized bond energy γ is related to its dimensional counterpart $\bar{\gamma}$, by

† More generally, γ may be considered to be an implicit function of α^*. In this event the functional Γ is defined in terms of its first variation $\delta\Gamma = 2\gamma \, \delta\alpha^*$ (i.e., the virtual work of the generalized force γ).

$$\gamma = \bar{\gamma} R^2 / \bar{D}.$$

The normalized interfacial stresses σ_1, σ_2 and τ (i.e., the Lagrange multipliers) are related to their dimensional counterparts in a manner analogous to that of the pressure.

We next invoke the Principle of Stationary Potential Energy which, in the present context, may be stated as

$$\delta \Pi = 0, \tag{12}$$

where δ corresponds to the variational operator.

Taking the appropriate variations, allowing the interior boundaries α and β to vary along with the displacements, we arrive at the correponding differential equations, boundary and matching conditions, and transversality conditions (the conditions which establish values of the "moveable" interior boundaries α and β, to be found as part of the solution together with the associated displacement field, which correspond to equilibrium configurations of the evolving structure). After eliminating the Lagrange multipliers from the resulting equations, we arrive at a self-consistent set of equations, and conditions (including energy release rates) for the evolving composite structure. We thus have

$$M_i^{*''} + M_i^{*} - (N_i^{*} w_i^{*'})' - N_i^{*} = -p, \quad N_i^{*'} = 0, \quad (\theta \in S_i; i = 1, 2) \tag{13a,b}$$

$$M_3'' + M_3 - (N_3 w_3')' - N_3 = -p, \quad N_3' = 0, \quad (\theta \in S_3) \tag{14a,b}$$

$$M_{p3}'' + M_{p3} - (N_{p3} w_{p3}')' - N_{p3} = 0, \quad N_{p3}' = 0, \quad (\theta \in S_{3p}) \tag{15a,b}$$

with

$$w_i^{*}(\theta) \equiv w_i(\theta) = w_{pi}(\theta), \quad (\theta \in S_i; i = 1, 2) \tag{16a,b}$$

$$\kappa_i^{*}(\theta) \equiv \kappa_i(\theta) = \kappa_{pi}(\theta), \quad (\theta \in S_i; i = 1, 2) \tag{16c,d}$$

$$u_1^{*}(\theta) = u_{p1}^{*}(\theta), \quad (\theta \in S_1) \tag{16e}$$

where

$$N_i(\theta) = C e_i(\theta) \quad \text{and} \quad N_{pi}(\theta) = C_p e_{pi}(\theta) \quad (i = 1-3) \tag{17a,b}$$

are the normalized resultant membrane forces in the base panel and patch, respectively, in region $S_i (i = 1-3)$,

$$N_1^{*}(\theta) = C^{*} e_1^{*}(\theta) + B^{*} \kappa_1^{*}(\theta) = N_1 + N_{p1}, \tag{18a}$$

$$M_1^{*}(\theta) = A^{*} \kappa_1^{*}(\theta) + B^{*} e_1^{*}(\theta) = D^{*} \kappa_1^{*}(\theta) + \rho^{*} N_1^{*}, \tag{18b}$$

respectively correspond to the normalized membrane force and normalized bending moment in the bonded portion of the composite structure,

$$N_2^{*}(\theta) = N_2 + N_{p2}, \quad M_2^{*}(\theta) = D_c \kappa_2^{*}(\theta) + \left(\frac{h_p}{2} N_{p2} - \frac{h}{2} N_2 \right), \tag{19a,b}$$

respectively correspond to the normalized resultant membrane force and bending moment of the debonded portion of the composite structure in the contact zone, and

$$M_3(\theta) = D \kappa_3(\theta) - \frac{h}{2} N_3, \quad M_{p3}(\theta) = D_p \kappa_{p3}(\theta) + \frac{h_p}{2} N_{p3}, \tag{20a,b}$$

correspond to the bending moments in the base cylinder and patch segments, respectively, in the region of separation.

The stiffnesses of the composite structure defined by eqns (13), (18) and (19) are found, in terms of the stiffnesses and thicknesses of the substructures, as

$$A^* = D + D_p + (h/2)^2 C + (h_p/2)^2 C_p, \tag{21a}$$

$$B^* = (h_p/2) C_p - (h/2) C, \tag{21b}$$

$$C^* = C + C_p, \tag{21c}$$

$$D^* = A^* - \rho^* B^* = D_c + (h^*/2)^2 C_s, \tag{21d}$$

where:

$$\rho^* = B^*/C^*, \quad D_c = D + D_p, \quad h^* = h + h_p \quad \text{and} \quad C_s = CC_p/C^*. \tag{21e–h}$$

The quantity ρ^* is seen to give the radial location of the centroid of the composite structure with respect to the reference surface, D_c is the bending stiffness of the debonded segment of the composite structure in the contact zone, $h^* \ll 1$ is the normalized thickness of the composite structure and C_s is an effective (series) membrane stiffness.

The associated boundary and matching conditions obtained similarly take the forms:

$$u_1^*(0) = 0, \quad w_1^{*\prime}(0) = 0, \quad \text{and} \tag{22a,b}$$

$$[M_1^{*\prime} - N_1^* w_1^{*\prime}]_{\theta=0} = 0 \quad \text{(applied pressure or circumferential tension)} \tag{22c}$$

$$\text{or} \quad w_1^*(0) = 0, \quad \text{(three-point loading)} \tag{22c′}$$

$$u_1^*(\alpha) = u_2^*(\alpha) = u_{p2}^*(\alpha), \quad N_1^*(\alpha) = N_2^*(\alpha), \tag{23a,b,c}$$

$$w_1^*(\alpha) = w_2^*(\alpha), \quad w_1^{*\prime}(\alpha) = w_2^{*\prime}(\alpha), \tag{23d,e}$$

$$M_1^*(\alpha) = M_2^*(\alpha), \quad [M_1^{*\prime} - N_1^* w_1^{*\prime}]_{\theta=\alpha} = [M_2^{*\prime} - N_2^* w_2^{*\prime}]_{\theta=\alpha}, \tag{23f,g}$$

$$u_2^*(\beta) = u_3^*(\beta), \quad N_2(\beta) = N_3(\beta), \tag{24a,b}$$

$$u_{p2}^*(\beta) = u_{p3}^*(\beta), \quad N_{p2}(\beta) = N_{p3}(\beta), \tag{24c,d}$$

$$w_2^*(\beta) = w_3(\beta) = w_{p3}(\beta), \tag{24e,f}$$

$$w_2^{*\prime}(\beta) = w_3'(\beta) = w_{p3}'(\beta), \tag{24g,h}$$

$$M_2^*(\beta) = M_3(\beta) + M_{p3}(\beta), \tag{24i}$$

$$[M_2^{*\prime} - N_2^* w_2^{*\prime}]_{\theta=\beta} = [M_3' - N_3 w_3']_{\theta=\beta} + [M_{p3}' - N_{p3} w_{p3}']_{\theta=\beta}, \tag{24j}$$

$$N_{p3}(\Phi_p) = \kappa_{p3}(\Phi_p) = [M_{p3}' - N_{p3} w_{p3}']_{\theta=\Phi_p} = 0, \tag{25a,b,c}$$

$$u_3(\Phi) = 0 \quad \text{or} \quad N_3(\Phi) = T_0 (T_0 \text{ prescribed}), \quad \text{and} \tag{26a,a′}$$

$$w_3(\Phi) = 0, \quad \text{and} \quad w_3'(\Phi) = 0 \quad \text{or} \quad \kappa_3(\Phi) = 0, \quad \text{(applied pressure and tension)} \tag{26b,c,c′}$$

or

$$[M_3' - N_3 w_3']_{\theta=\Phi} = -Q_0 (Q_0 \text{ prescribed}) \quad \text{and} \quad \kappa_3(\Phi) = 0. \quad \text{(3-point loading)} \tag{26′b,c}$$

The transversality condition for the propagating bond zone boundary, $\theta = \alpha$, takes the following forms depending upon the presence or absence of a contact zone. Hence,

$$\mathcal{G}_{\mathscr{A}}\{\alpha\} \equiv \left[\tfrac{1}{2}D_c\kappa_2^{*2} + \frac{1}{2C}N_2^2 + \frac{1}{2C_p}N_{p2}^2\right]_{\theta=\alpha} - \left[\frac{1}{2}D^*\kappa_1^{*2} + \frac{1}{2C^*}N_1^{*2}\right]_{\theta=\alpha} = 2\gamma, \quad (\beta \geqslant \alpha^+) \tag{27a}$$

$$\mathcal{G}_{\mathscr{B}}\{\alpha\} \equiv \left[\frac{1}{2}D\kappa_3^2 + \tfrac{1}{2}D_p\kappa_{p3}^2 + \frac{1}{2C}N_3^2 + \frac{1}{2C_p}N_{p3}^2\right]_{\theta=\alpha} - \left[\frac{1}{2}D^*\kappa_1^{*2} + \frac{1}{2C^*}N_1^{*2}\right]_{\theta=\alpha} = 2\gamma, \quad (\beta = \alpha) \tag{27b}$$

where $\mathcal{G}_{\mathscr{A}}\{\alpha\}$ and $\mathcal{G}_{\mathscr{B}}\{\alpha\}$ are identified as the energy release rates. The conditions (27) suggest the following delamination criterion:

if, for some initial value of $\alpha = \alpha_0$, we have that $\mathcal{G}\{\alpha_0\} \geqslant 2\gamma$, then debonding occurs and the system evolves (α decreases—α^* increases) such that the corresponding equality (27a) or (27b) is satisfied. If $\mathcal{G}\{\alpha_0\} < 2\gamma$, debonding does not occur.

For a propagating contact zone boundary $\theta = \beta$, the associated transversality condition reduces to the form

$$\kappa_2^*(\beta) = \kappa_3(\beta) = \kappa_{p3}(\beta), \quad (\beta < \Phi_p) \tag{28a,b}$$

to which we add the qualification

$$\kappa_3(\beta^+) > \kappa_{p3}(\beta^+) \tag{28c}$$

to prohibit penetration of the base panel and path for $\theta \in S_{3p}$. It is thus seen that such a boundary is defined by the point where the curvature changes of the respective segments of the structure are continuous. The system (1)–(28) defines the class of problems of interest.

The boundary conditions (25), together with eqns (15a,b), indicate that the "flap" (i.e., the segment of the debonded portion of the patch which is lifted away from the base structure) is unloaded and hence that

$$N_{p3}(\theta) = \kappa_{p3}(\theta) = M'_{p3}(\theta) = 0. \quad (\forall\theta \in S_{3p}) \tag{29a,b,c}$$

Further, integration of eqns (13b) and (14b), imposition of the associated matching conditions (23c), (24b), and (24d), and incorporation of eqn (29a) yields the results

$$N_1^* = N_2 = N_3 = N_0 = \text{constant}, \quad N_{p2} = 0. \tag{30}$$

The remaining equations and conditions are modified accordingly, with the transversality conditions (27)–(28) taking the forms

$$\mathcal{G}_{\mathscr{A}}\{\alpha\} \to \left[\frac{1}{2}D_c\kappa_2^{*2} - \tfrac{1}{2}D^*\kappa_1^{*2} + \frac{1}{2C_c}N_0^2\right]_{\theta=\alpha} = 2\gamma, \quad (\beta \geqslant \alpha^+) \tag{27'a}$$

$$\mathcal{G}_{\mathscr{B}}\{\alpha\} \to \left[\frac{1}{2}D\kappa_3^2 - \tfrac{1}{2}D^*\kappa_1^{*2} + \frac{1}{2C_c}N_0^2\right]_{\theta=\alpha} = 2\gamma, \quad (\beta = \alpha) \tag{27'b}$$

and

$$\kappa_2^*(\beta) = \kappa_3(\beta) = 0, \quad \kappa_3(\beta^+) > 0, \quad (\beta < \Phi_p) \tag{28'a,b,c}$$

where:

$$1/C_c \equiv \frac{(C_p/C)}{C^*}. \tag{31}$$

It may be seen from eqn (28′) that a propagating or intermediate contact zone boundary may occur only if conditions are such that an inflection point occurs in the interval $\alpha < \theta < \Phi_p$. If not, the system will possess either a full contact zone ($\beta = \Phi_p$), or no contact zone ($\beta = \alpha$). For the former case, the lifted segment of the flap (region S_{3p}) will not exist, and the condition

$$\kappa_2(\alpha^+) < 0 \quad (\beta = \Phi_p) \tag{28″a,b}$$

must be satisfied.

Integrating the strain-displacement relations and imposing the corresponding boundary and matching conditions for the circumferential displacements results in the *integrability condition* given by

$$u_3(\Phi) = N_0\left[\frac{\alpha^*}{C} + \frac{\alpha}{C^*}\right] - \left[\frac{h}{2} + \rho^*\right]w'(\alpha) + \sum_{i=1}^{3}\int_{S_1}((1-\rho^*\delta_{i1})w_i - \tfrac{1}{2}w_i'^2)\,\mathrm{d}\theta, \tag{32}$$

where δ_{ij} is Kronecker's delta. The counterparts of eqns (13a) and (14a) and the corresponding boundary and matching conditions obtained upon substitution of the results (29) and (30), together with the transversality conditions (27′) and (28′), and the integrability condition (32), transform the problem statement into a mixed formulation in terms of the transverse displacement $w_i(\theta)$ ($i = 1$–3), the membrane force N_0, and the moving boundaries α and β.

3. ANALYSIS

We next present the basis of a linear analysis of the problems of interest based on the formulation presented in the previous section. As in Bottega (1995) we first examine the existence of a contact zone.

Contact zone

Upon substitution of the linearized version of eqn (13a) into the corresponding equation for the patch in region 2 (not presented), we arrive at an expression for the corresponding (radially directed) interfacial stress, σ_2, given by

$$\sigma_2 = -(p - N_0)D_p/D_c. \tag{33}$$

When contact between the surfaces of the base panel and the patch occurs, the contact stress will necessarily be "compressive" (i.e., $\sigma_2 < 0$). It may be seen from eqn (33) that $\sigma_2 \geqslant 0$ when $p = 0$ ($N_0 \geqslant 0$), from which it may be concluded that a contact zone does not exist for the cases under consideration where the applied pressure vanishes. For non-vanishing pressure it is seen that when $p > N_0$, the contact stress is compressive and hence that a contact zone may exist for the case of pressure loading. Further contingencies regarding the presence of an intermediate or propagating contact zone concern the magnitudes and signs of the curvatures of the composite structure and substructures as specified by eqns (28′a–c) as discussed at the end of the previous section. Additionally, if an inflection point does not occur on the interval $[\alpha, \Phi_p]$ then a "full contact zone" ($\beta = \Phi_p$) will be present (the entire debonded segment of the patch will be in sliding contact with the base panel) provided conditions are such that $\kappa_2(\alpha^-) < 0$. If these conditions are not met either, then no contact zone exists for the pressure loaded case as well.

Evolving structure

Paralleling the analysis of Bottega (1995) for similarly configured flat structures, we first define the normalized loading parameter λ and characteristic deflection Δ, for each of the specific problems (applied tension, 3-point radial loading, and applied pressure), respectively, as follows:

$$\{\lambda = T_0, \Delta = u_3(\Phi)\}; \quad \{\lambda = Q_0, \Delta = w_3(\Phi)\}; \quad \{\lambda = p, \Delta = -w_1(0)\}. \quad (34a\text{–}c)$$

We shall also define the "global stiffness" for each particular problem as

$$K \equiv \lambda/\Delta, \quad (35)$$

for each (λ, Δ) pair defined in eqn (34).

Since we shall perform a linear analysis, the response in each case will be found to be proportional to the loading parameter for the specific problem under consideration. The integrability condition (32) will then take the general form

$$u_3(\Phi) = \lambda \mathscr{F}_\lambda(\alpha) + N_0 \mathscr{F}_N(\alpha), \quad (36)$$

where $\mathscr{F}_\lambda(\alpha)$ and $\mathscr{F}_N(\alpha)$ are functions obtained by substituting the specific analytical solution for the transverse displacement into eqn (32). For problems where $\lambda = T_0$, we have, from condition (26a′), that $N_0 = T_0$. Equation (36) then gives the normalized circumferential edge displacement as a function of the applied tension for this case. For other loading types, eqn (36) gives the normalized membrane force N_0 as a function of λ for fixed end conditions ($u(\Phi) = 0$), and gives the circumferential edge displacement as a function of λ for free edge conditions, where $N_0 = 0$ from eqn (26a′).

For each case and for each increment in load, the particular equilibrium configuration of the evolving system has associated with it a particular value of the contact zone boundary β for a given value of α. It was established in the previous subsection that $\beta = \alpha$ for both the case of applied circumferential tension and the case of three-point radial loading. For the case of internal pressure loading, however, we must first seek a value of $\beta : \alpha < \beta < \Phi_p$ such that eqns (28′a–c) are satisfied. If no such β can be found, then either $\beta = \alpha$ or $\beta = \Phi_p$. The latter can only occur if the kinematic condition $\kappa_2(\alpha^+) < 0$ is satisfied. If this condition is not satisfied either, then $\beta = \alpha$.

With the above established, the energy release rates can be written in terms of the loading parameter explicitly, for each case under consideration. The equations for the growth paths/ threshold curves λ vs α (or α^*) and Δ vs α (or α^*) may then be found directly from the transversality conditions (27′), and take the general forms

$$\lambda^* \equiv \lambda\sqrt{2\gamma} = 1/\sqrt{\Omega(\alpha; S, \beta)}, \quad \Delta^* \equiv \Delta/\sqrt{2\gamma} = K^{-1}(\alpha; S, \beta)/\sqrt{\Omega(\alpha; S, \beta)}, \quad (37a,b)$$

where $\Omega(\alpha; S, \beta)$ is the normalized energy release rate per square of the normalized load, S is the set of stiffnesses of the structure, and (λ^*, Δ^*) correspond one to one with each (λ, Δ) pair defined earlier in this section. In this way, the evolution of the debonding structure may be characterized using the analytical solution for each particular problem of interest. Results for specific configurations are presented in the next section.

4. RESULTS AND DISCUSSION

In this section, results are presented for the following loading types: (1) applied circumferential tension, (2) three-point radial loading, and (3) applied (internal) pressure. In each case analytical solutions for the corresponding problem based on a linearization of the formulation presented in Section 2 are employed to generate the corresponding threshold curves and stiffness degradation curves. In what follows, we consider the specific base

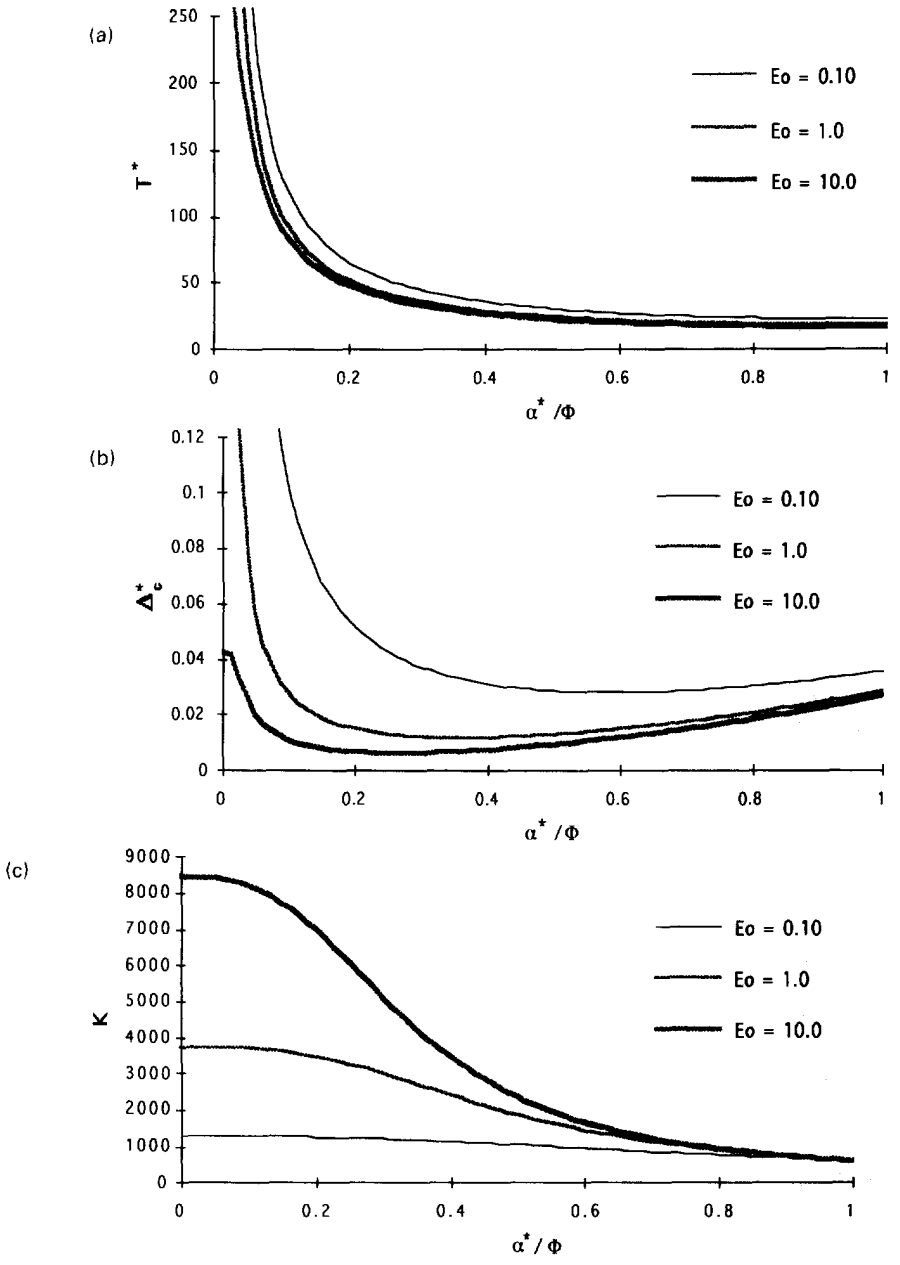

Fig. 3. Theshold curves/delamination paths for patched panel under applied circumferential tension for the case of hinged-free supports: (a) normed applied tension vs conjugate bond zone size, (b) normed circumferential edge deflection vs conjugate bond zone size, (c) global stiffness as a function of conjugate bond zone size.

structure of half-span $\Phi = 0.4$ and normalized thickness $h = 0.02$, with a patch such that $h_p = h$, for the modulus ratios $E_0 = 0.1$, 1.0, and 10.0. With the exception of the case of three-point radial loading, the effect of the support conditions on the behavior of the evolving structure is examined. Results corresponding to each loading type are discussed separately.

4.1. *Applied circumferential tension*

Results corresponding to the curve where a circumferentially directed tensile load of normalized magnitude T_0 is applied to the base structure at the edges $\theta = \pm\Phi$ are displayed in Figs 3–4 and presented in the form of plots of the renormed load $T^* = T_0/\sqrt{2\gamma}$, renormed circumferential edge displacement $\Delta_c^* = u_3(\Phi)/\sqrt{2\gamma}$, and global stiffness $K = T^*/\Delta_c^*$, as functions of the conjugate bond zone boundary α^*. The loaded edge is considered to be

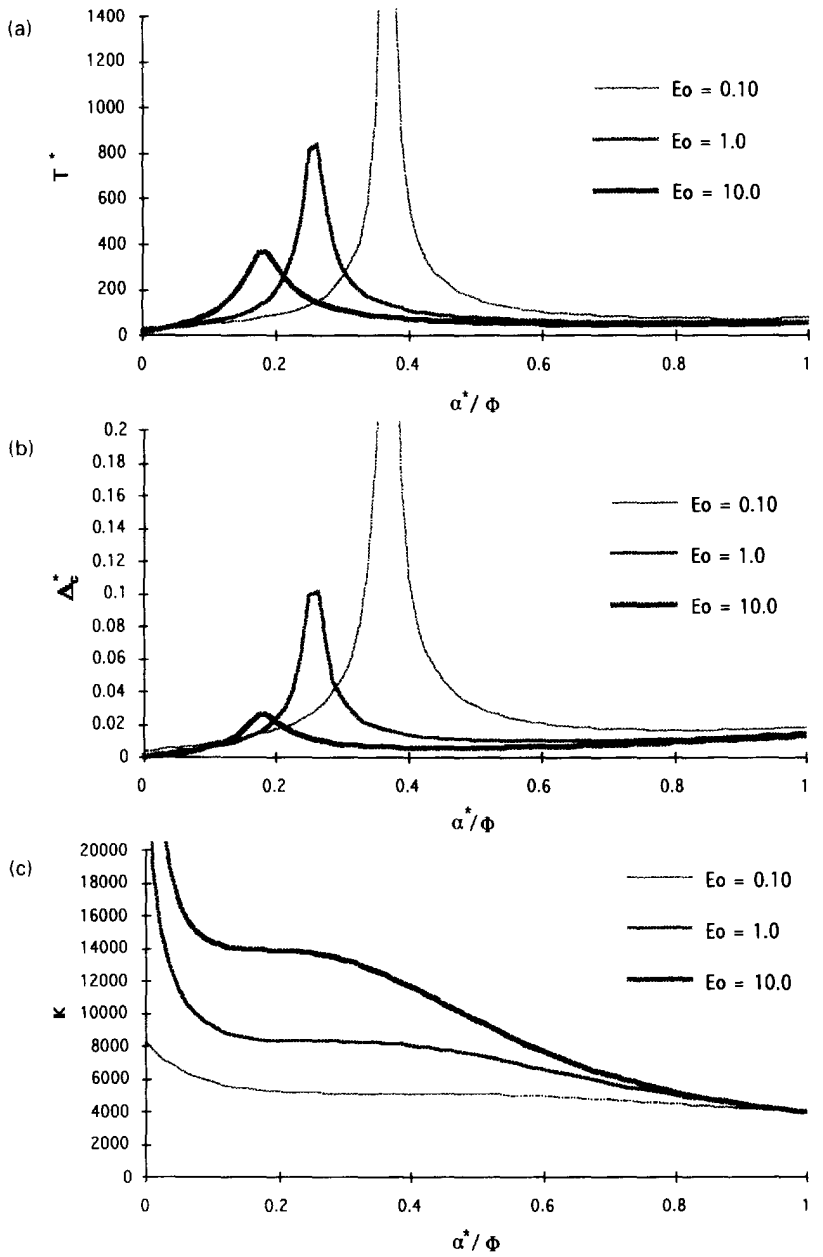

Fig. 4. Threshold curves for patched panel under applied circumferential tension for the case of clamped-free support conditions: (a) normed applied tension vs conjugate bond zone size, (b) normed circumferential edge deflection vs conjugate bond zone size, (c) global stiffness as a function of conjugate bond zone size.

free to translate circumferentially, and either hinged (free to rotate) or clamped (fixed against rotation). As discussed in the first part of Section 3, a contact zone does not exist for the given structure under this type of loading. Examination of the results corresponding to hinged supports, Figs 3a–c, shows that debonding occurs in an unstable and catastrophic manner for force controlled loading. However, under displacement controlled loading, the results indicate that debonding may occur in a catastrophic manner, or in a stable manner depending upon the initial size of the bonded region. Thus, critical conjugate bond zone sizes characterize the ensuing behavior of the debonding structure for displacement controlled loading. The corresponding degradation of the global stiffness K is represented in Fig. 3c. It is seen that patches with greater stiffnesses debond at lower load levels than their more compliant counterparts.

While the general behavior for the case of hinged supports is seen to be qualitatively similar to the corresponding behavior indicated for the analogous problem concerning flat structures (Bottega, 1995), the results for the case of clamped supports displayed in Figs 4a–c differ substantially from their counterparts for flat structures. Examination of the threshold curves for the case of clamped supports shows similar behavior for both force controlled (Fig. 4a) and displacement controlled (Fig. 4b) loading. In each case, it is seen that relatively large bond zones (relatively small α^*) separate in a stable manner initially until the indicated peak is reached, at which point catastrophic debonding occurs. For bond zones whose initial conjugate bond size is beyond the peak, debonding characteristics are qualitatively similar to those for displacement controlled loading for the case of hinged supports. That is debonding occurs in a catastrophic manner, in an unstable followed by a stable manner, or in a stable manner depending upon the initial size of the bonded region.

4.2. *Three-point radial loading*

We next present results for the case where the structure is supported by a knife edge at centerspan and is subjected to an inwardly directed radial point/line load of normalized intensity Q_0 applied at each edge, $\theta = \pm\Phi$, of the base panel. The edges are considered to be free to translate and to rotate. As for the case of applied circumferential tension, the discussion of the first part of Section 3 indicates that no contact zone exists for the present case. Results are presented in the form of threshold curves in terms of the renormed load intensity $Q^* = Q_0/\sqrt{2\gamma}$ and renormed radial edge displacement $\Delta_\Phi^* = w_3(\Phi)/\sqrt{2\gamma}$ as a function of the conjugate bond zone boundary, α^*, in Figs 5a and 5b while the degradation of the global stiffness of the structure, $K = Q^*/\Delta_\Phi^*$, is presented in Fig. 5c. It is seen that, as for the analogous problem concerning flat structures (Bottega, 1995), debonding under force controlled loading occurs in a catastrophic manner, while it occurs in a stable manner, in an unstable followed by a stable manner, or in a catastrophic manner, depending on the initial size of the bonded region, when the deflections are controlled.

4.3. *Applied (internal) pressure*

The behavior of a patched cylindrical panel subjected to applied internal pressure will be examined for both the case of hinged supports and the case of clamped supports. For each type of support pertaining to rotation we will also consider the effects of fixing or freeing the supports with regard to circumferential translation. We thus consider "hinged-free" and "hinged-fixed" support conditions, and "clamped-free" and "clamped-fixed" support conditions. We shall consider the case of hinged support conditions first.

Hinged supports. Threshold and stiffness degradation curves for the case of hinged-free support conditions are displayed in Figs 6a–c, while those for the case of hinged-fixed support conditions are presented in Figs 7a–c. As for the analogous problems concerning flat structures (Bottega, 1995), no contact zone was found for these cases. Consideration of Fig. 6a, which displays the threshold value of the renormed pressure $p^* = p/\sqrt{2\gamma}$ as a function of the conjugate bond zone size, shows that debonding occurs in a catastrophic manner for force controlled loading. The threshold curves for the corresponding characteristic deflection $\Delta_0^* = -w(0)/\sqrt{2\gamma}$ indicate that, for the case of deflection controlled loading, debonding occurs in a catastrophic, unstable followed by stable, or stable manner depending upon the initial value of the conjugate bond zone size. The corresponding stiffness degradation curves are displayed in Fig. 6c, where $K = p^*/\Delta_0^*$. If the base panel is fixed with regard to circumferential translation at the support (hinged-fixed), thus introducing a resultant circumferential tension in the base panel, the corresponding behavior is seen to be stabilized somewhat as indicated by the threshold curves shown in Figs 7a and 7b and the associated stiffness degradation curves of Fig. 7c. Thus, the system is seen to behave in an unstable followed by a stable manner or in a stable manner for both force and deflection controlled loading situations, depending upon the initial size of the bonded region. Catastrophic failure is indicated only for patches which are initially bonded over almost the entire span of the base structure, for the case of force controlled loading, and in addition only for the case of a relatively compliant patch for the case of deflection controlled

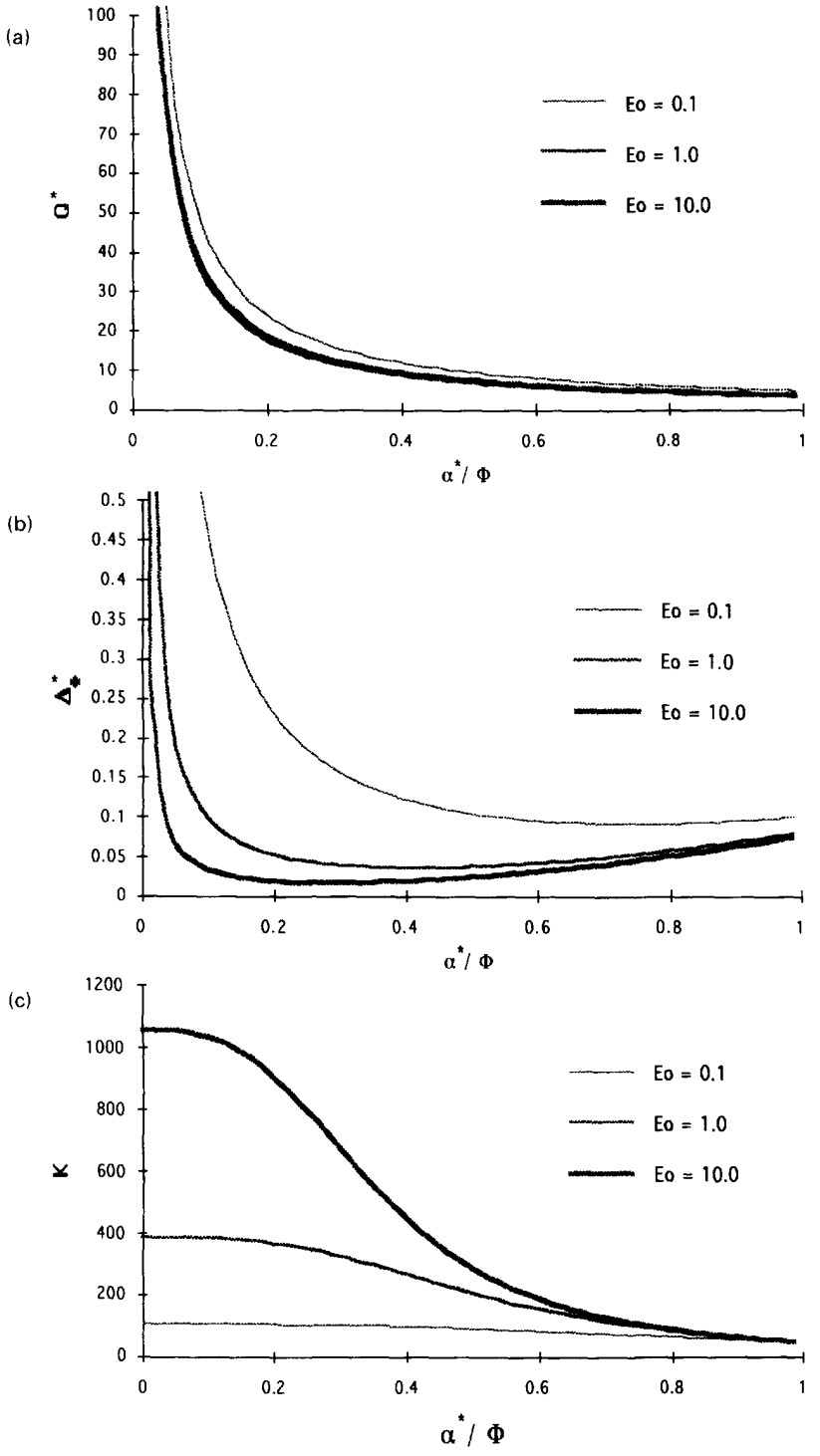

Fig. 5. Threshold curves/delamination paths for patched panel under radial three-point loading: (a) normed load intensity vs conjugate bond zone size, (b) normed radial edge deflection vs conjugate bond zone size, (c) global stiffness as a function of conjugate bond zone size.

loading. In all cases it is seen that the stiffer patches debond at lower load levels than their more compliant counterparts. It may be seen from Fig. 7c that the "global stiffness" actually increases slightly, over a range of α^*, as the damage progresses for the patches with modulus ratios $E_0 = 0.1$ and $E_0 = 1.0$. This misleading tendency occurs because the global stiffness is characterized as the ratio of the pressure to the deflection at a single point—the center of the span of the structure. For the cases indicated, the behavior of the composite structure

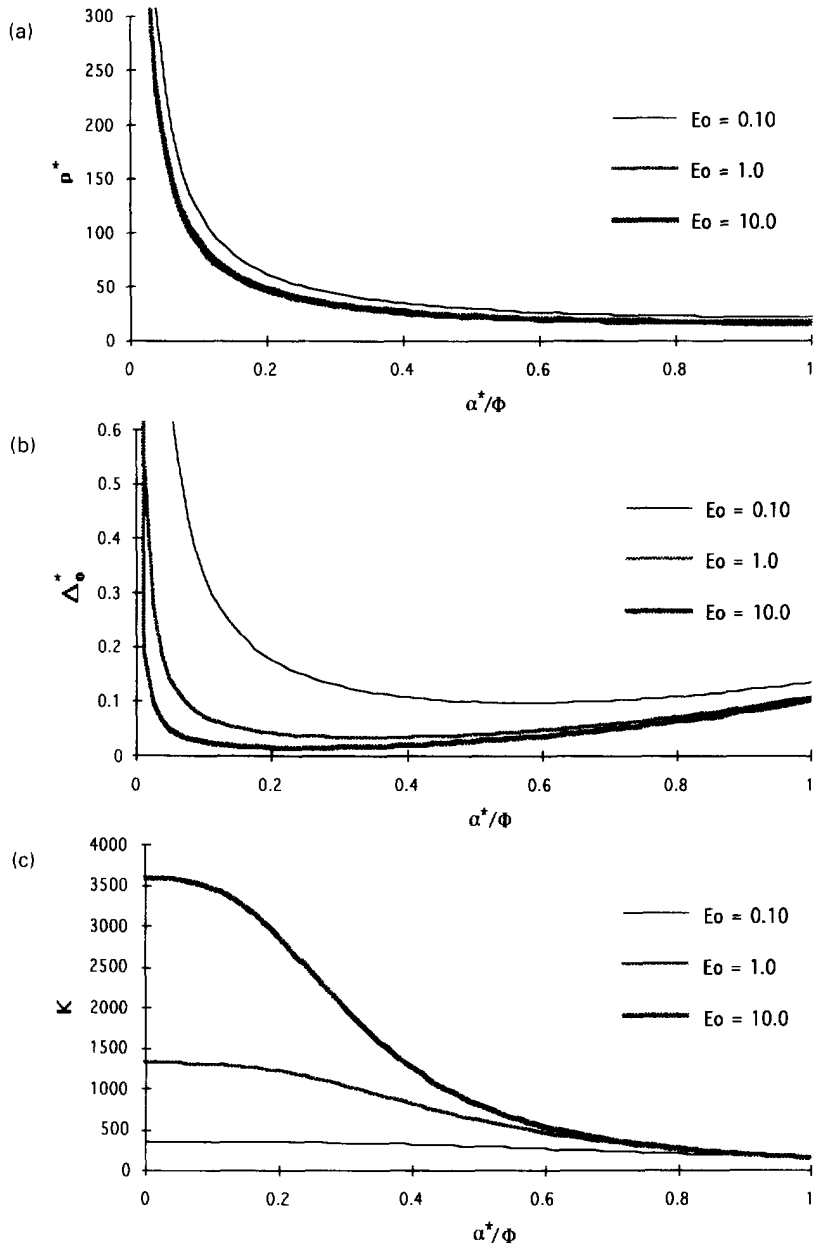

Fig. 6. Threshold curves/delamination paths for patched panel under applied (internal) pressure for the case of hinged-free support conditions: (a) normed applied pressure vs conjugate bond zone size, (b) normed radial centerspan deflection vs conjugate bond zone size. (c) global stiffness as a function of conjugate bond zone size.

is such that much of the deformation occurs in the base panel within the region of separation. This is demonstrated for the case of a bond zone of half-length $\alpha = 0.7$ ($\alpha^* = 0.3$) in Fig. 8, where the transverse deflection of the entire (half) span is shown as a function of the conjugate angular coordinate $\theta^* \equiv \Phi - \theta$ (the distance from the supported edge) at the threshold level.

Clamped supports. In this last case, we consider the evolution of the structure when the edge supports are clamped so as to prohibit rotation. Both the case where the base panel is free to translate circumferentially (clamped-free supports) and the case where the base panel is restricted from translating circumferentially (clamped-fixed supports) are considered. Unlike, any of the other cases considered to this point, the system is found to possess a full contact zone ($\beta = \Phi_p$) for relatively long patches which are bonded over a

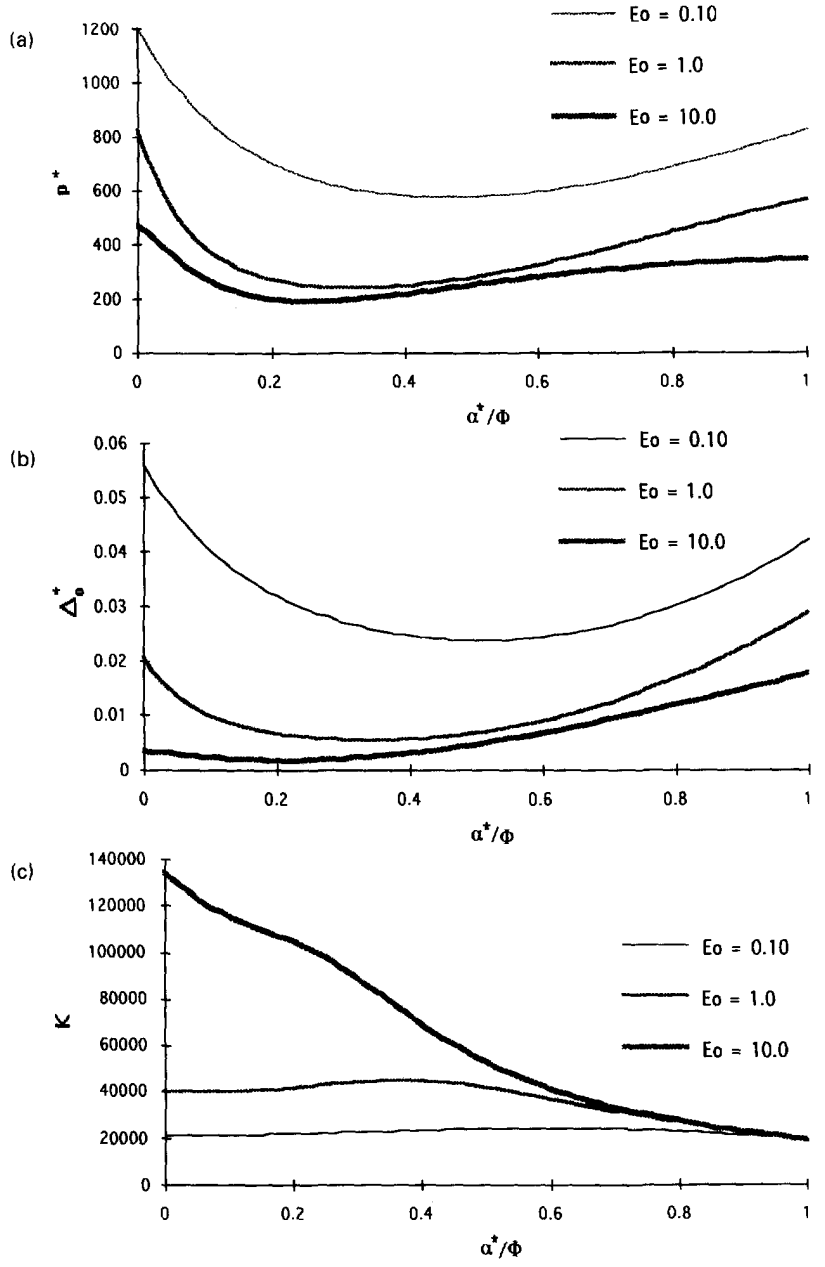

Fig. 7. Threshold curves/delamination paths for patched panel under applied (internal) pressure for the case of hinged-fixed support conditions: (a) normed applied pressure vs conjugate bond zone size, (b) normed radial centerspan deflection vs conjugate bond zone size, (c) global stiffness as a function of conjugate bond zone size.

sufficient portion of the span. Intermediate contact zones ($\alpha < \beta < \Phi_p$) are not, however, observed.

Figures 9a, b and 10a, b show the threshold curves for the case of clamped-free support conditions when the debonding structure possesses a *full contact zone*. Figure 9 depicts results for the specific patch size of relative length $\Phi_p/\Phi = 0.9$ and compares the threshold curves for various modulus ratios E_0. Each path shown is seen to be asymptotic and is cut off near its limiting value of α^*. It is thus seen that patches of these relative lengths, which are initially bonded over most of the span of the base structure, debond in a stable manner and ultimately arrest. Such behavior is typical of relatively long patches as indicated by the threshold curves shown in Figs 10a and b. In these figures the delamination paths corresponding to various relative patch lengths, $\Phi_p/\Phi = 1.0, 0.9, 0.8$, are displayed for the

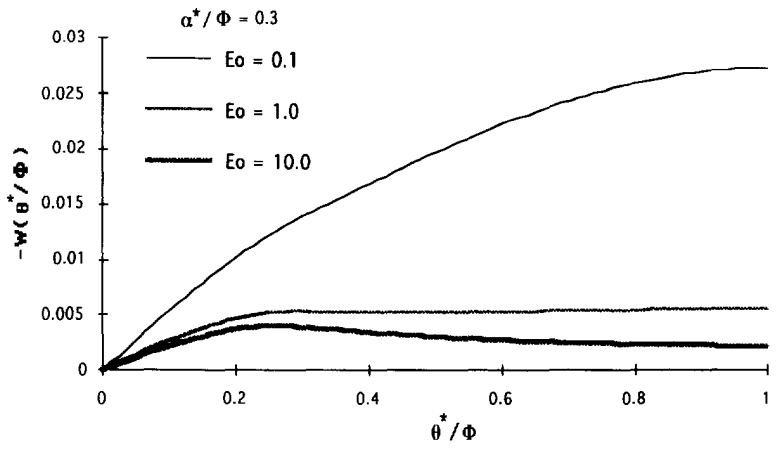

Fig. 8. Radial deflection of entire half-span of composite structure under applied pressure, at threshold level, as a function of relative angular distance from support for conjugate bond size $\alpha^* = 0.3$, for the case of hinged-fixed supports.

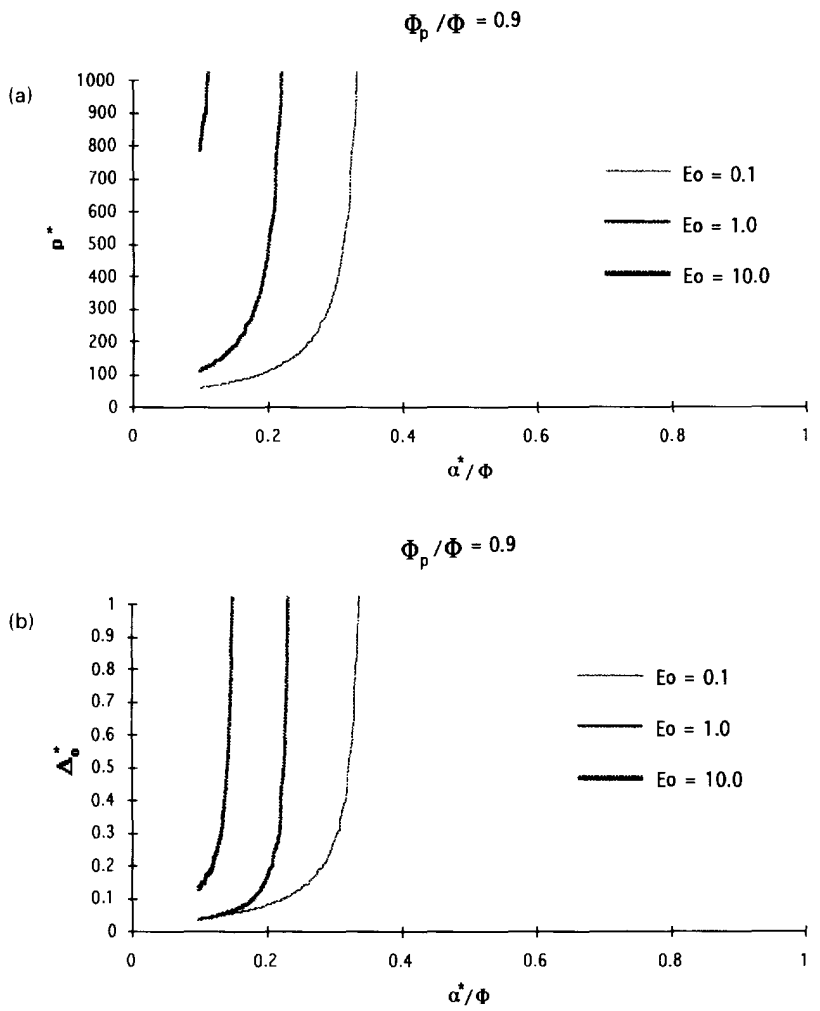

Fig. 9. Full contact zone threshold curves for patched panel under applied (internal) pressure for the case of clamped-free supports and $\Phi_p/\Phi = 0.9$: (a) normed pressure vs conjugate bond zone size, (b) normed radial centerspan deflection vs conjugate bond zone size.

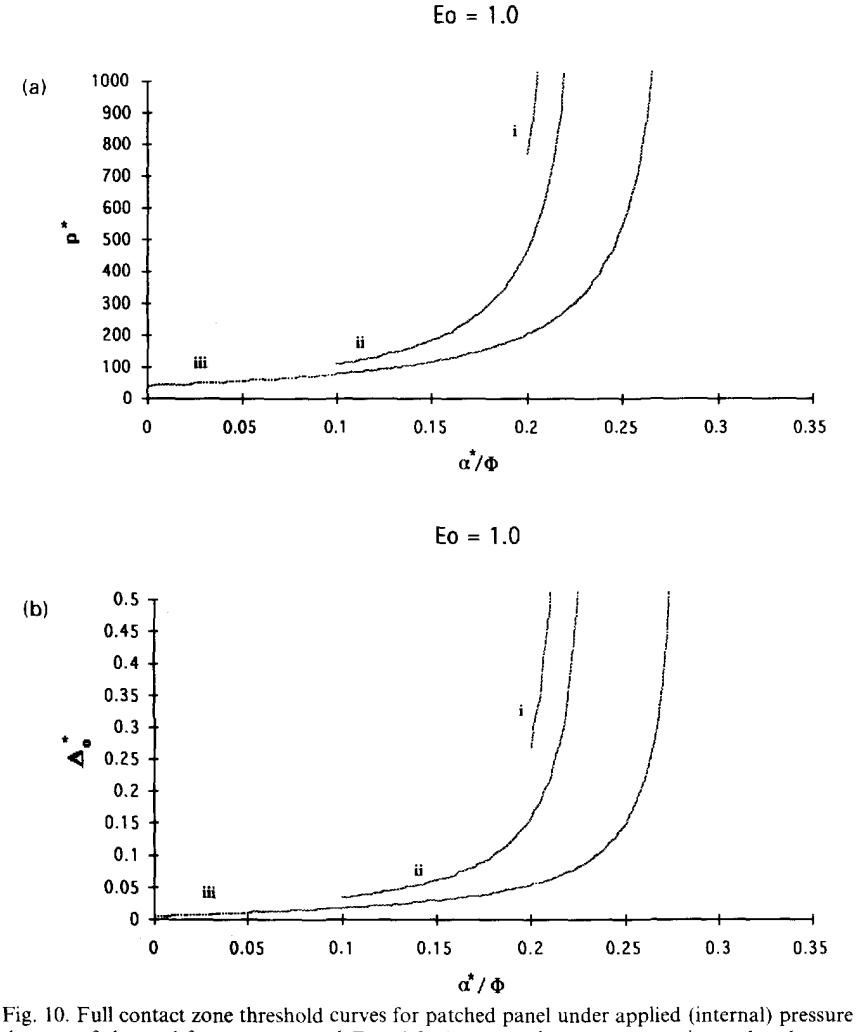

Fig. 10. Full contact zone threshold curves for patched panel under applied (internal) pressure for the case of clamped-free supports and $E_0 = 1.0$: (a) normed pressure vs conjugate bond zone size, (b) normed radial centerspan deflection vs conjugate bond zone size. In each, labels correspond to: (i) $\Phi_p/\Phi = 0.8$, (ii) $\Phi_p/\Phi = 0.9$, (iii) $\Phi_p/\Phi = 1.0$.

case of unit modulus ratio ($E_0 = 1.0$). For this case, patches of lengths $\Phi_p/\Phi < 0.78$ possess no contact zone at all. The corresponding threshold curves for the case of no contact zone are presented in Figs 11a and b, where each path is seen to approach an asymptote†. It is thus seen that the behavior of the evolving structure for patches whose initial conjugate bond size is greater than this asymptotic value is qualitatively similar to that for the case of hinged-free supports discussed earlier. That is, debonding occurs in a catastrophic manner for pressure controlled loading, and in a catastrophic, unstable followed by stable, or in a stable manner for deflection controlled loading. The corresponding behavior of the system differs, somewhat, when the supports are fixed against translation as well as rotation (clamped-fixed) as indicated by the curves presented in Figs 12–15.

Threshold curves corresponding to configurations where the structure possesses a full contact zone are displayed in Figs 12 and 13, while those corresponding to the situation of no contact zone are displayed in Figs 14a–c along with the associated stiffness degradation curves. As for the parallel studies pertaining to similarly configured flat structures (Bottega, 1995), contact zones are seen to be present for relatively long patches which are bonded over most of their (arc) length, only. Figure 12 shows the delamination paths for a patch

† A companion asymptotic branch of each curve is found for values of α^* to the left of the corresponding asymptote. These branches are not shown, however, since they are, in general, never achieved due to the presence of a full contact zone as indicated by the results shown in Figs 9 and 10.

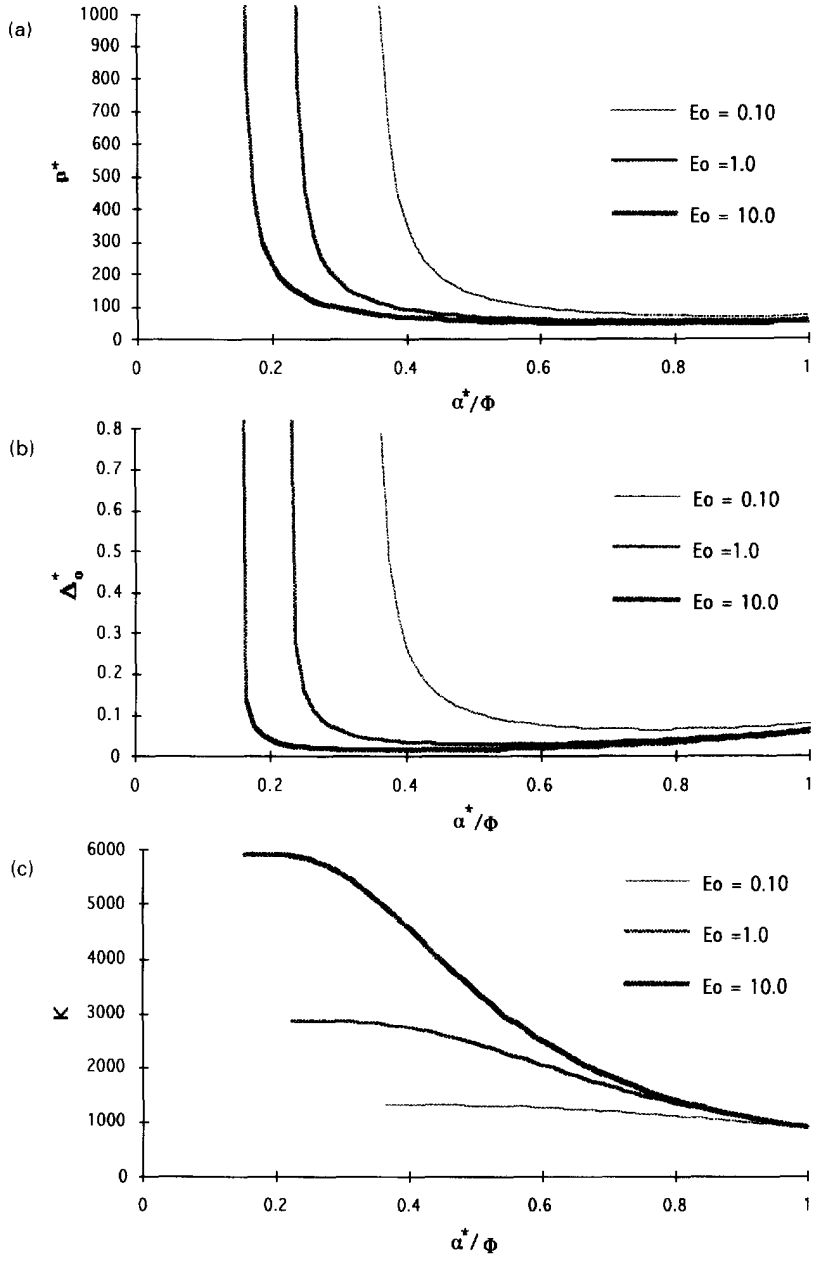

Fig. 11. Vanishing contact zone threshold curves for patched panel under applied (internal) pressure for the case of clamped-free supports: (a) normed pressure vs conjugate bond zone size, (b) normed radial centerspan deflection vs conjugate bond zone size, (c) global stiffness vs conjugate bond-zone size.

which covers the entire base panel ($\Phi_p/\Phi = 1.0$) for the modulus ratios $E_0 = 0.1$ and $E_0 = 1.0$, when the system possesses a full contact zone. As for the corresponding study involving similarly configured flat structures (Bottega, 1995), no contact zone is found for the relatively stiff patch ($E_0 = 10.0$). Full contact zone paths corresponding to patches of various sizes ($\Phi_p/\Phi = 1.0, 0.9, 0.8$) are shown in Figs 13a and b for $E_0 = 0.1$. The paths in both Figs 12 and 13 are seen to approach asymptotes separating stable and unstable debonding, the exception being the path corresponding to $E_0 = 1.0$ for the case where $\Phi_p/\Phi = 1.0$ of Fig. 12 (which exhibits an unstable branch only—the asymptote and stable branch being shifted out of the range of allowable values of α^*). In addition, the threshold curves for patches which are short enough are seen to only possess an unstable branch, as seen in Fig. 13 for $\Phi_p/\Phi = 0.8$. Thus, relatively long patches that are initially bonded over

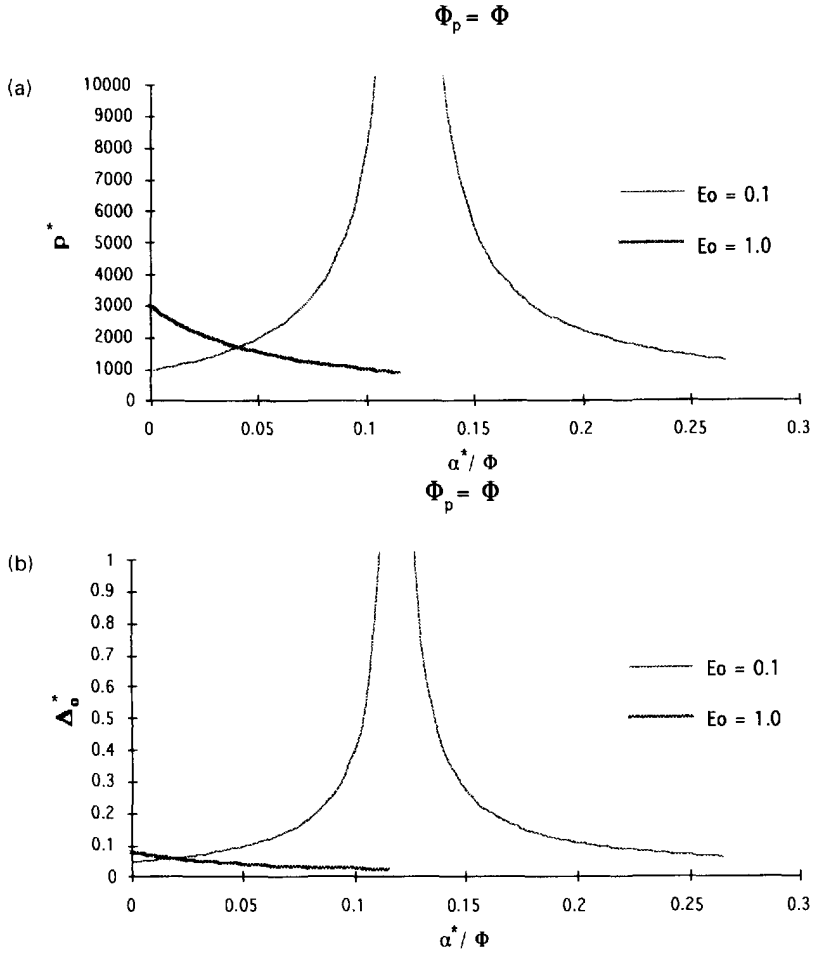

Fig. 12. Full contact zone threshold curves for patched panel under applied (internal) pressure for the case of clamped-fixed supports and $\Phi_p/\Phi = 1.0$: (a) normed pressure vs conjugate bond zone size, (b) normed radial centerspan deflection vs conjugate bond zone size.

most of their length are seen to exhibit stable debonding, and to ultimately effectively arrest, with α^* approaching the corresponding asymptotic value, as the pressure (or characteristic displacement) is increased. Similarly configured "long" patches with smaller initial bond zones (α^* to the right of the corresponding asymptote) are seen to debond in an unstable manner once the threshold level of the pressure (displacement) is achieved. Once initiated, unstable debonding continues until the cutoff point of the path is achieved at which point the contact zone ceases to exist. Debonding is then described by the paths displayed in Fig. 15 and is seen to be catastrophic. As the full contact zone paths (Figs 12 and 13) lie above the corresponding paths for no contact zone (Fig. 14), patches with initial conjugate bond zone sizes to the right of the asymptote are seen to debond catastrophically once the threshold level is achieved. (The two paths are superimposed in Fig. 15, for the case where $E_0 = 0.1$ and $\Phi_p/\Phi = 1.0$.) This behavior can be explained as follows; as discussed in section 3 of this paper, the presence or absence of a contact zone is dependent upon the presence and location of an inflection point and/or the signs of the curvature changes across the bond zone boundary. For the case of the stiff patch ($E_0 = 10.0$), the most severe deformation occurs in the unbonded portion of the base structure, hence the inflection point never occurs in the bonded region. With regard to the more compliant patches; for relatively large bond zones, an inflection point occurs within the bonded region of the structure and the curvature changes of the base panel and composite structure at either side of the bond zone boundary are both negative, and hence a full contact zone is present. For the case of the compliant patch ($E_0 = 0.1$) the deformation is such that the inflection point is sufficiently far from the

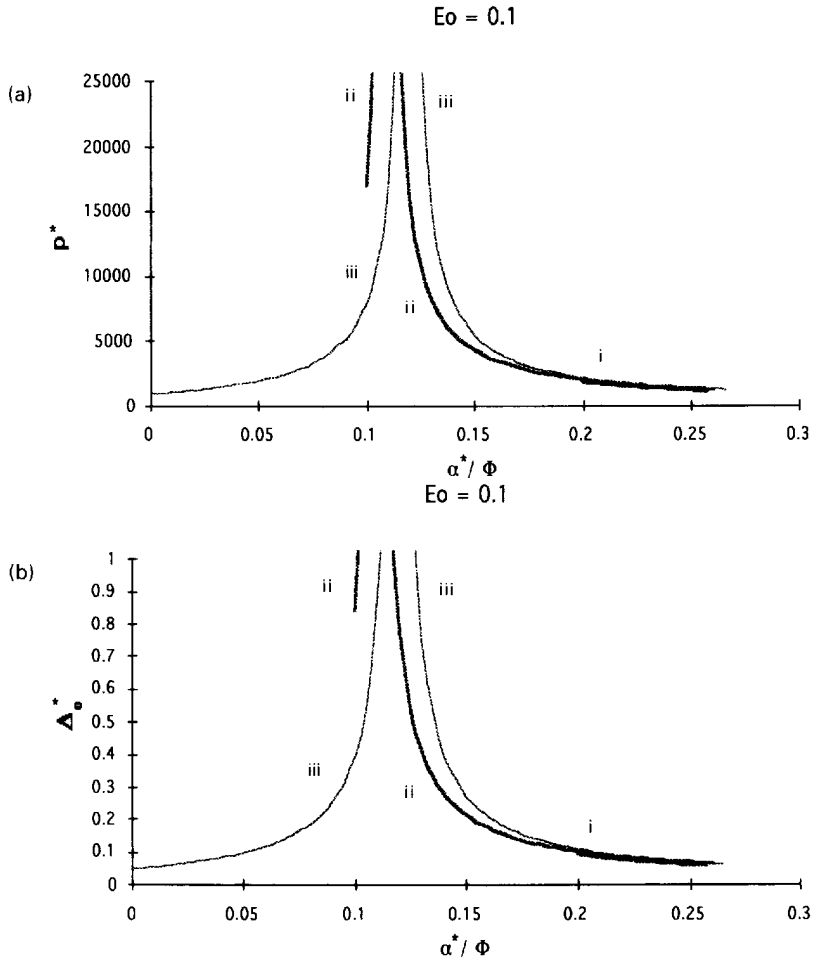

Fig. 13. Full contact zone threshold curves for patched panel under applied (internal) pressure for the case of clamped-fixed supports and $E_0 = 0.1$: (a) normed pressure vs conjugate bond zone size, (b) normed radial centerspan deflection vs conjugate bond zone size. In each, labels correspond as : (i) $\Phi_p/\Phi = 0.8$, (ii) $\Phi_p/\Phi = 0.9$, (iii) $\Phi_p/\Phi = 1.0$.

bond zone boundary and so becomes "trapped" for large enough bond zones, and debonding is ultimately arrested. For slightly smaller bond zones this is not the case, nor is it so for the intermediate patch ($E_0 = 1.0$). For these cases, as unstable debonding of the patch from the base panel progresses in the direction away from the edge of the structure, the inflection point moves toward the bond zone boundary until it encroaches upon it. At this point the jump in curvature change across $\theta = \alpha$ is such that a contact zone cannot exist and the debonded flap "lifts off" from the base panel. When this occurs, delamination ensues via eqn (27'b) and the system debonds catastrophically. For patches with initial bond zone sizes small enough (α^* large enough) such that a contact zone does not exist initially, it is seen from Fig. 14 that the debonding process is stable or perhaps unstable followed by stable for both pressure controlled or deflection controlled loading, with the exception of the case of $E_0 = 0.1$ where it is seen that structures initially possessing relatively large bond zones will debond catastrophically.

4.4. *Comments on the influence of delamination modes for transverse loading*

With regard to the influence of delamination modes, we consider the possibility that the debonding scenarios discussed may be altered somewhat if the delamination mode ratio (or "crack loading phase") varies radically and in a suitable fasion, as the bond zone boundary propagates under interface conditions in which "mode mixity" (see, for example, Hutchinson and Suo, 1992) is an issue. This may be seen not to be the case, however, for

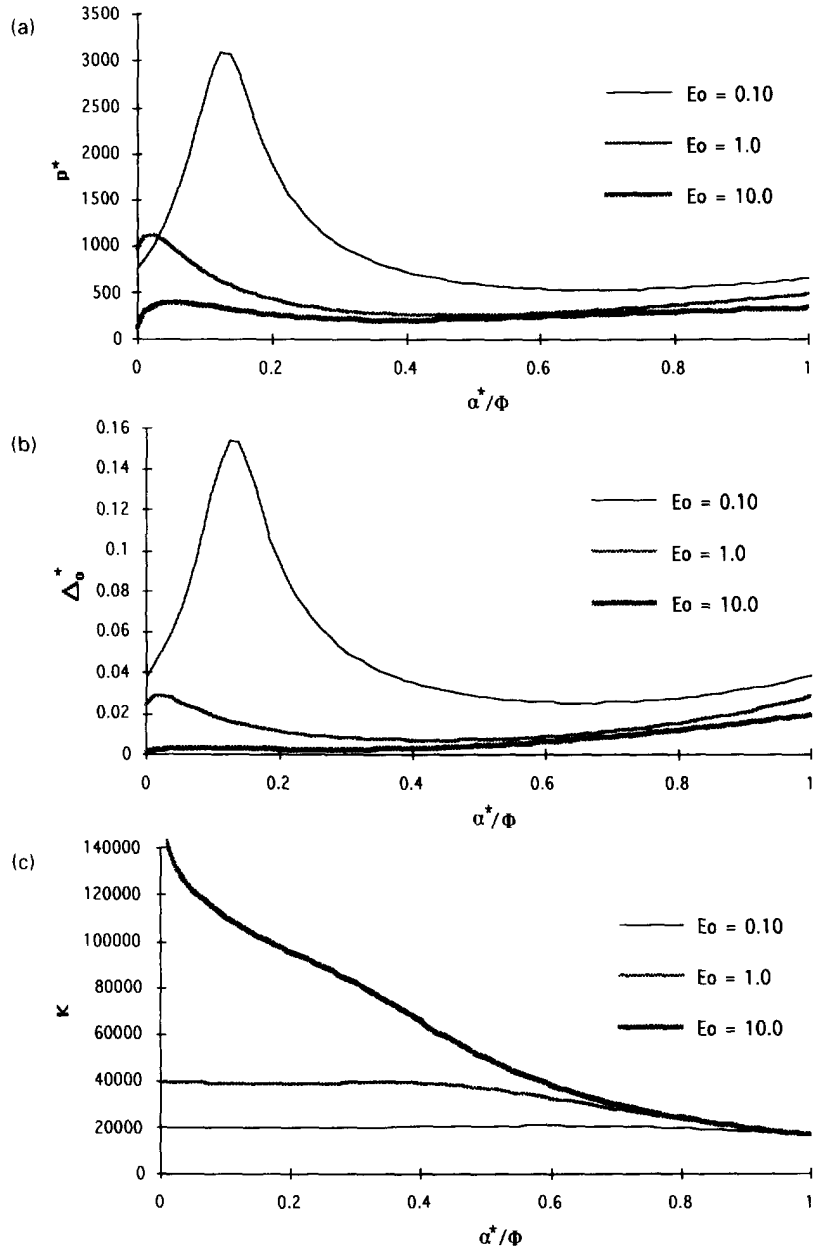

Fig. 14. Vanishing contact zone threshold curves for patched panel under applied (internal) pressure for the case of clamped-fixed supports: (a) normed pressure vs conjugate bond zone size, (b) normed radial centerspan deflection vs conjugate bond zone size, (c) global stiffness vs conjugate bond-zone size.

the loading cases considered, even for the dramatic transition from mode-II dominated debonding with a contact zone to debonding without a contact zone observed for the case of the pressure loaded panel with clamped-fixed supports. Calculations of the "large scale" interfacial stresses (see Appendix A) show $\sigma_1(\alpha)$ to be compressive and $\tau(\alpha)$ to maintain the same sign for all α, and both $\sigma_1(\alpha)$ and $\tau(\alpha)$ to vary smoothly with α, for each case when a contact zone is not present. Similarly, $\sigma_1(\alpha)$ and $\tau(\alpha)$ are found to vary smoothly with α, with $\tau(\alpha)$ maintaining the same sign, when a contact zone is present. However, for the case of clamped-fixed supports, the shear (and $\sigma_1 \ll |\tau|$) is in the opposite sense as that when the contact zone is absent. Thus there is a "shear reversal" when "lift off" occurs for this case. If σ_1 and τ are considered to represent the "distant loading" (or some average measure)

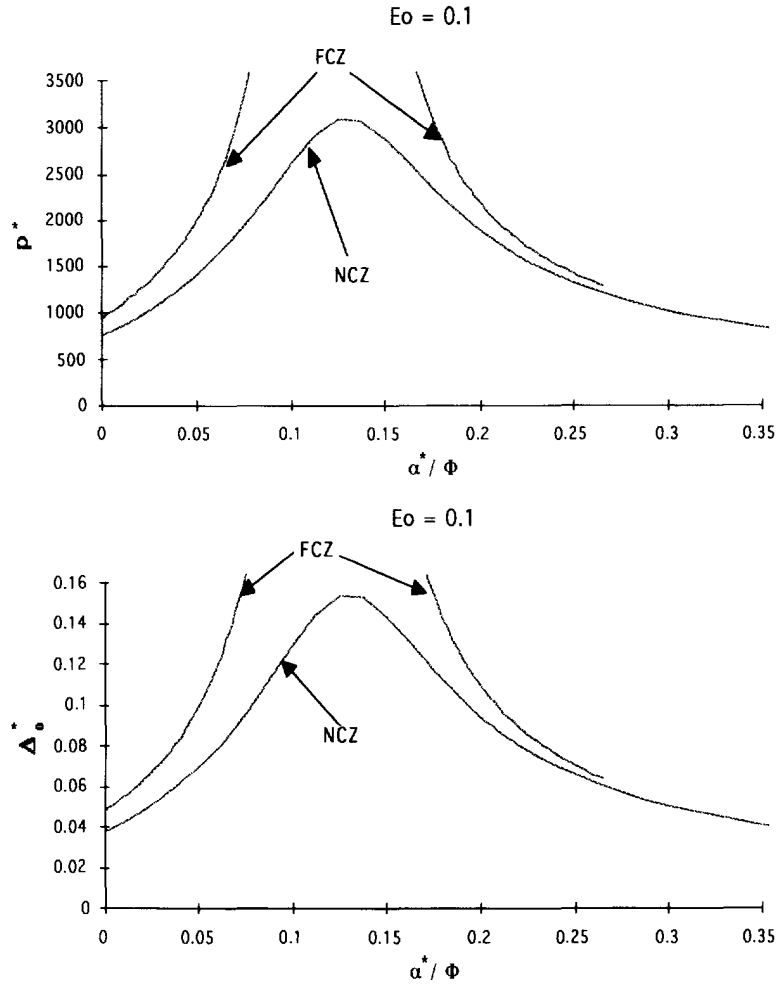

Fig. 15. Comparison of threshold curves for vanishing and nonvanishing contact zone for patched panel under applied pressure for the case of clamped-fixed supports and $E_0 = 0.1$.

with regard to local small scale effects, then their characteristics appear to support the notion that the local ("small scale") stress field, and hence the local mode ratio/phase, varies smoothly with α (or maintains pure mode-II) as well, for these cases. If this is so, and in view of the above, it is anticipated that the delamination modes have little influence on the debonding scenarios discussed for the particular loading conditions considered.

5. CONCLUDING REMARKS

The problem of edge debonding in patched cylindrical panels has been considered for a variety of loading and support conditions. It was seen that the manner of support may significantly affect the debonding behavior of the composite structure. It was observed, for the loading conditions considered, that a contact zone may exist for the case of applied internal pressure and that the presence or absence of such a contact zone is dependent upon the relative length of the patch and the corresponding relative stiffness of the patch. Such a contact zone was seen not to propagate and hence to cover the entire span of the debonded segment of the patch, unlike the more complex behavior observed for related studies concerning debonding in cylindrical structures (Bottega, 1988a–d, 1994, and Loia and Bottega, 1994). In all cases considered, debonding was seen to occur in one or in a combination of several ways; stable, stable followed by arrest, unstable followed by stable, or catastrophic. As for the case of flat structures, debonding was seen to ensue at lower load levels for stiffer patches.

To conclude, it was seen that nonvanishing initial curvature of the structure influences the debonding behavior of the class of structures considered.

Acknowledgement—The authors wish to thank D. W. Oplinger of the Federal Aviation Administration for his support and encouragement. This work was supported by the FAA through the Rutgers University Center for Computational Modeling of Aircraft Structures (CMAS).

REFERENCES

Baker, A. A. (1993). Repair efficiency in fatigue-cracked aluminum components reinforcred with boron/epoxy patches. *Fatigue Fract. Engng Mat. Struct.* **16,** 753–765.

Bottega, W. J. (1983). A growth law for propagation of arbitrary shaped delaminations in layered plates. *Int. J. Solids Structures* **19,** 1009–1017.

Bottega, W. J. (1988a). On thin film delamination growth in a contracting cylinder. *Int. J. Solids Structures* **24,** 13–26.

Bottega, W. J. (1988b). Peeling of a cylindrical layer. *Int. J. Fracture* **38,** 3–14.

Bottega, W. J. (1988c). Debonding of a predeflected segment of layer from the wall of a contracting cavity. *Engng Fract. Mech.* **31,** 1001–1008.

Bottega, W. J. (1988d). On delamination of thin layers from cylindrical surfaces. In *Proceedings of the 29th AIAA/ASME/ASCE/AHS Structures, Structural Dynamics and Materials Conference*, Williamsburg, pp. 351–358.

Bottega, W. J. (1994). On circumferential splitting of a laminated cylindrical shell. *Int. J. Solids Structures* **31,** 1891–1909.

Bottega, W. J. (1995). Separation failure in a class of bonded plates. *Comput. Struct.* **30,** 253–269.

Chiu, W. K., Rees, D., Chalkey, P., and Jones, R. (1994). Designing for damage-tolerant composite repairs. *Comp. Struct.* **28,** 19–37.

Chue, C.-H., Chang, L.-C., and Tsai, J.-S. (1994). Bonded repair for a plate with inclined central crack under Biaxial loading. *Comp. Struct.* **28,** 39–45.

Hutchinson, J. W. and Suo, Z. (1992). Mixed mode cracking in layered materials. *Advances in Applied Mechanics*, Vol. 29 (eds J. W. Hutchinson and T. Y. Wu), Academic Press, San Diego, pp. 63–191.

Loia, M. A. and Bottega, W. J. (1994). Blister growth in layered cylinders. *Comp. Engng* **4,** 1275–1287.

Oplinger, D. W. (1994). Effects of adherend deflections in single lap joints. *Int. J. Solids Structures* **31,** 2565–2587.

Park, J. H., Ogiso, T., and Atluri, S. N. (1992). Analysis of cracks in aging aircraft structures, with and without composite-patch repairs. *Computer Mech.* **10,** 169–201.

Paul, J., and Jones, R. (1992). Repair of impact damaged composites. *Engng Fract. Mech.* **41,** 127–141.

Roderick, G. L. (1980). Prediction of cyclic growth of cracks and debonds on aluminum sheets reinforced with boron/epoxy. In *Fibrous Composites in Structural Design* (eds E. M. Lenoe, D. W. Oplinger, and J. J. Burke), Plenum Press, New York, pp. 467–481.

Schellekens, J. C. J. and de Borst, R. (1993). A non-linear finite element approach for the analysis of mode-I free edge delamination in composites. *Int. J. Solids Structures* **30,** 1239–1253.

Sih, G. C. and Hong, T. B. (1989). Integrity of edge-debonded patch on cracked panel. *Theor. Appl. Fract. Mech.* **12,** 121–139.

Tarn, J.-Q., and Shek, K.-L. (1991). Analysis of cracked plates with a bonded patch. *Engng Fract. Mech.* **40,** 1055–1065.

Tsai, M.-Y., and Morton, J. (1994). A note on peel stresses in single-lap joints. *ASME J. Appl. Mech.* **61,** 712–715.

APPENDIX: BOND ZONE STRESSES

The expressions for the interfacial stresses (Lagrange multipiers) $\tau(\theta)$ and $\sigma_1(\theta)$, $\theta \in S_1$, are found from the equations for the primitive structures in region S_1 (not presented) together with the corresponding equations for the composite structure, eqns (13a,b) for $i = 1$, along with eqns (17), (18a) and (30). After some manipulation it is found that

$$\tau(\theta) = -C\left(\rho^* + \frac{h}{2}\right)\kappa_1'(\theta) \tag{A1}$$

and

$$\sigma_1(\theta) = -\frac{D_p}{D^*}[p - N_0(1-\rho^*)] - \frac{h_p}{2}\tau'(\theta) - \frac{C_p}{C^*}\left[N_0 + \frac{h^*}{2}C\kappa_1(\theta)\right]\left(1 - \frac{h_p}{2}\right). \tag{A2}$$